Journal of the Korean Nuclear Society
Volume 25, Number 3, September 1993

An Experimental Study of Direct Containment Heating Phenomena

Chanyoung Chung and Gyoodong Jeun
Hanyang University

Kwang Hyun Bang and Moohwan Kim
Pohang Institute of Science and Technology

(Received March 11, 1993)

격납용기 직접가열 현상에 관한 실험적 연구

정찬영 · 전규동
한양대학교

방광현 · 김무환
포항공과대학

(1993. 3. 11 접수)

Abstract

This paper reports an experimental study of direct containment heating (DCH) which would occur if the primary system pressure is still high at the time of vessel breach during a light water reactor core melt accident. The experiments were conducted in 1/30-scale cavity models of Kori unit 1 and 2 and Young Kwang unit 3 and 4 nuclear power plants. One 1/20-scale model of the Kori plant was also used to investigate the scaling effect. The primary variables in the experiments were initial vessel pressure, vessel breach size and cavity geometry. It is observed that higher initial pressure and larger breach size enhance the melt dispersal fraction. Also, the cavity geometry appears to affect the dispersal rate greatly. A simple correlation of melt dispersal fraction is proposed in terms of nondimensional effective period. This correlation shows good agreement with the present experimental data, the KAIST data and the BNL data.

요 약

본 논문에서는 경수로 노심 용융사고시 1차계통의 압력이 높은 경우에 발생하는 격납용기 직접가열 현상에 대한 실험연구를 하였다. 실험은 고리 1,2호기와 영광 3,4호기의 1/30 축소규모와 고리 1,2호기의 1/20 축소규모를 실험모형으로 하여 수행되었으며, 고리 1,2호기의 경우 축소 규모에 따른 검증도 시도하였다. 실험의 주요 변수는 초기 압력 용기의 압력, 파열면적 및 캐비티의 구조 등이다. 실험결과로부터 캐비티 외부로의 용융노심 분사비율은 높은 초기압력과 큰 파열면적을 가진 경우가 더 높으며 캐비티의 구조가 분사비율에 큰 영향을 미침을 알 수 있었다. 본 연구의 실험결과를 이용하여 분사비율에 대한 실험관계식을 무차원 유효시간의 함수로 도출하여 제시하였으며, 이 실험관계식은 본 실험결과 뿐만 아니라 한국 과학기술원의 실험자료 및 미국 BNL 실험결과와도 잘 일치하였다.

1. Introduction

In the present day light water reactors (LWRs), if complete and prolonged failure of normal and emergency coolant flow occurs, fission product decay heat could cause melting of the reactor fuel. If the molten fuel mass is relocated and accumulates on the lower head of the reactor pressure vessel (RPV), it could cause the lower head to fail by a thermally induced rupture or by expulsion of an incore instrument guide tube. If the reactor coolant system (RCS) is still at high pressure at the time of this lower head failure, forcible melt ejection and blowdown of the RCS into the reactor cavity is initiated.

Blowdown gas adds both mass and energy to the containment atmosphere. Some portions of the molten material that is ejected into the reactor cavity can be entrained, fragmented and dispersed into the containment atmosphere. The debris dispersed from the reactor cavity can rapidly liberate its thermal energy to the containment atmosphere. The metallic components of the dispersed material can oxidize with steam, releasing both energy and hydrogen. These processes will heat the containment atmosphere and are, in general, called 'direct containment heating(DCH)', which might lead to early failure of the reactor containment building by overpressurization or overheating. The current probabilistic safety assessments (PSA) of nuclear power plants are being extended to include severe accident phenomena such as DCH.

The past research on DCH phenomena have been both experimental and analytical. An experimental study was conducted at Argonne National laboratory using a 1/40-scale Zion cavity in order to investigate a threshold gas velocity of the melt dispersal process [1]. In this study, they applied the observed fluid removal criteria to the reactor system and suggested that water should be swept from the cavity if the steam/gas velocity in the tunnel exceeds 10 m/sec, and if higher than 30 m/sec, both the melt and water should be dispersed. A scaling analysis and a series of experiments were also performed at Brookhaven National laboratory using three 1/42 linear scale cavity models of Zion, Surry and Watts-Bar plants [2, 3]. They identified the breakup of melt jet by dissolved gas, atomization at the vessel breach, splash and entrainment from liquid film as the mechanisms of droplets formation of the dispersed melt. They also proposed a scaling analysis using a group of nondimensional parameters.

In Sandia National laboratory, a series of experiments have been carried out using 1/10 linear scale cavity of Zion plant [4, 5]. In this study, the aerosol characteristics of melt debris and the effects of water and cavity structure were investigated and the effect of flying distance of melt droplets in the containment was examined. Their results indicated that water had little effect on DCH phenomena while cavity structure had a significant effect. It appears that the use of high temperature melt simulant and larger scale model makes these experiments unique in DCH studies. Recently, Lee [6] and So [7] at KAIST added a data set from the tests using Woods metal and water. They used 1/41 and 1/25-scale cavities of Young Kwang Unit 1 and 2. They observed that the melt dispersal fraction is higher in the larger scale cavity. However, the cut-off pressure for the melt dispersal is nearly identical in both scales.

In the analytical part of DCH studies, one-dimensional control-volume analyses were performed by a number of researchers [8, 9, 10] in support of experimental data analysis and severe accident analysis. In these analyses, the DCH effects were quantified based on global mass and energy balances. In addition, three-dimensional models have been developed to investigate the flow of the melt and driving gases.

This paper reports a systematic experimental in-

vestigation of the key parameters in melt dispersal process that have been identified in the past studies. These are cavity geometry, initial RCS pressure and volume, and the size of vessel breach. The primary purpose of the present study is to understand the key parameters in the dispersal mechanism and to develop a simple correlation of melt dispersal fraction in terms of nondimensional parameters. For this purpose, water was chosen as a melt simulant and three different scaled cavities were used.

2. Experimental Apparatus

A schematic diagram of the experimental apparatus is shown in Fig. 1. It consists mainly of a gas tank, melt holder, solenoid ball valve, and cavity. The gas tank is connected to the melt holder by a 19.4 mm ID steel pipe and it simulates the reactor coolant system. The melt holder is made of stainless steel and it initially contains melt simulant. The total gas volume of the gas tank and melt holder is determined based on the linear scale from the corresponding reactor coolant system volume as listed in Table 1. The melt holder is connected to the cavity by a ball valve. It is initially closed to maintain the high pressure in the melt holder and it is opened by fast solenoid actuation to simulate the vessel breach. The vessel breach

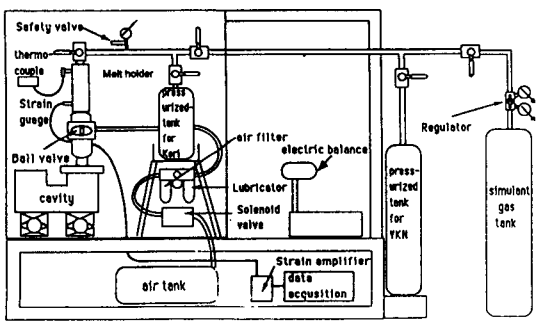

Fig. 1. A Schematic Diagram of Experimental Apparatus

size is varied by an orifice with a circular hole located between the ball valve and the cavity. The three orifice sizes used in this study are 10, 15, and 20 mm in diameter. A thin aluminum foil is layered at the orifice and it ruptures at the applied pressure as the ball valve is opened. This orifice unit is enclosed and connected to the cavity by a large tube fitting nut. The cavity is made of transparent acrylic for visual observation. The three cavity models used in this study are 1/20-scale and 1/30-scale cavities of Kori Unit 1 and 2 and 1/30-scale cavity of Young-Kwang unit 3 and 4. A schematic of these cavities is shown in Fig. 2 with the key dimensions.

The initial pressure and temperature of the melt

Table 1. Summary of Initial Conditions and Geometric Dimensions

Initial Conditions	Experimental Cavity Model		
	Kori 1/20th	Kori 1/30th	YKN 1/30th
Pressure of the primary System (MPa)	0.50-1.91	0.30-1.60	0.52-2.60
Containment Pressure (MPa)	0.1	0.1	0.1
Mass of the Core Melt Simulant (kg)	1.044	0.310	0.471
Temperature of the Core Melt (K)	300	300	300
Temperature of the Driving Gas (K)	300	300	300
Volume of the Driving Gas (m^3)	0.0228	0.0112	0.0112
Diameter of the Breach Size (mm)	10/15/20	10/15/20	10/15/20

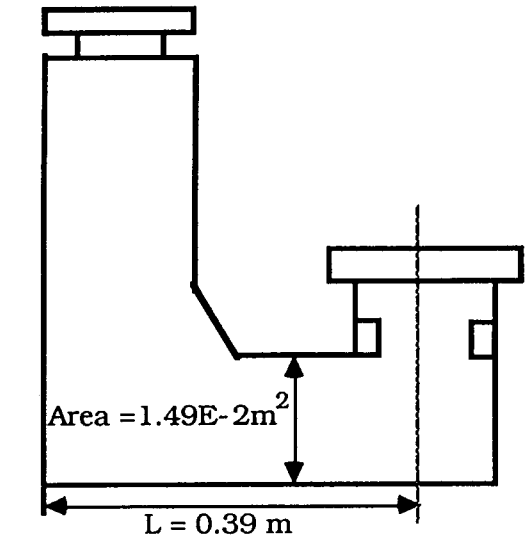

(1) Young-Kwang unit 3, 4
1/30th scaled cavity

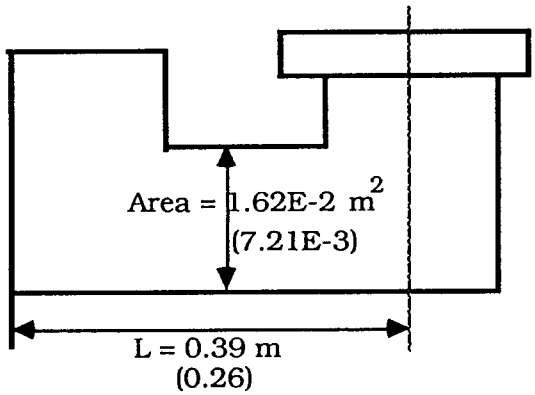

(2) Kori unit 1,2 1/20 scaled cavity

* ( ) ; Kori 1/30th scaled

Fig. 2. Shape and Dimensions of Cavity Models

and gas in the melt holder are measured using a dynamic strain gauge and thermocouples. This pressure transducer also allows the measurement of pressure trace in the melt holder during the blowdown phase. The flow visualization of the cavity is made by a high speed camera. The dispersed amount of the melt from the cavity is measured by the difference of the initial melt mass and the remaining mass in the cavity after the test. The mass of the melt is measured using an electric balance.

3. Results and Data Analysis

A series of tests were conducted using water as a melt simulant and three cavity models. The driving gas was primarily nitrogen, but helium or carbon dioxide was also used in selected tests in order to examine an effect of the type of simulant gas. The primary experimental parameters were cavity geometry and scale, breach size, and vessel pressure. The initial conditions and the key variables are summarized in Table 1.

3.1. Parametric Effects on Melt Dispersal Fraction

The measured fractions of the melt dispersed from the cavity are shown in Fig. 3 to Fig. 5 for each cavity model as a function of initial vessel pressure and breach size. It is seen that there is a cut–off pressure below which no melt is dispersed from the cavity. This cut–off pressure appears to depend upon the scale and breach size in these tests. The dispersal fraction increases as the pressure increases and approaches to the maximum of about 80% within the current experimental range.

It is also observed that the larger breach size (orifice diameter) enhances the melt dispersal fraction and this trend is more apparent in the data of Kori 1/20–scale and Young–Kwang cavities. This may be attributed to the magnitude of gas velocity in the cavity tunnel; as the ratio of the tunnel flow area to the breach size becomes larger the velocity of blowdown gas gets smaller in the tunnel where the entrainment of melt droplets takes place. This observation was taken into account in the data analysis which will be discussed in sec-

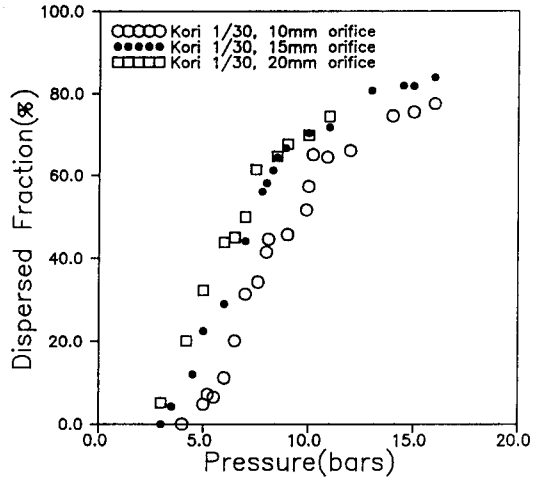

Fig. 3. Dispersed Fraction vs. Initial Vessel Pressure in Kori 1/20-scale

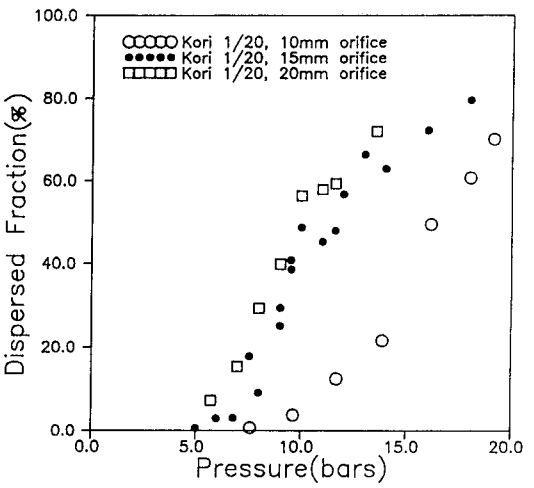

Fig. 5. Dispersed Fraction vs. Initial Vessel Pressure in YKN1/30-scale

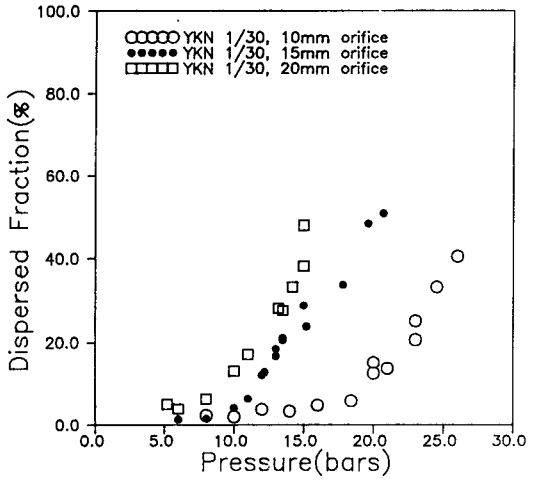

Fig. 4. Dispersed Fraction vs. Initial Vessel Pressure in Kori 1/30-scale

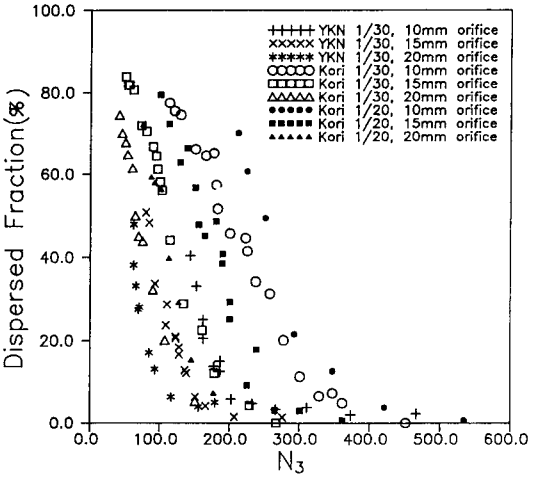

Fig. 6. Dispersed Fraction vs. Nondimensional Number N_3

tion 3.3.

The effect of cavity geometry is shown in Fig. 4 and Fig. 5 using the data of 1/30-scale cavities of Kori and Young-Kwang plants. The smaller dispersal fraction in Young-Kwang cavity is due primarily to the longer flight length of the droplets in the cavity tunnel since the length of the tunnel in Young-Kwang cavity is 50% longer than Kori cavity as shown in Fig. 12. It takes longer in Young-Kwang cavity for the entrained droplets to exit the cavity. This flight length and gas velocity in the cavity are considered as the key parameters

in the formulation of dispersal fraction correlation which will be presented in section 3.3.

3.2. Nondimensional Analysis

The parameters which have the main effect on the dispersal mechanism are blowdown time, drag force on the melt film at the cavity wall, and the force of breaking melt drops. In order to present the experimental results with these factors, four nondimensional numbers were selected from the work of Tutu et al. [2].

$$N_3 = \frac{\sigma}{\mu_g u_R} \tag{1}$$

$$N_4 = \frac{P_0 V_0^*}{P_\infty} \tag{2}$$

$$N_5 = \frac{\rho_R u_R^2}{\sqrt{\rho_L g \sigma}} \tag{3}$$

$$N_6 = \frac{\frac{\mu_L u_R}{\sigma}\sqrt{\frac{\rho_R}{\rho_L}}}{N_\mu^{0.8}} \tag{4}$$

where,

$$N_\mu = \frac{\mu_L}{\sqrt{\rho_L \sigma \sqrt{\frac{\sigma}{\rho_L g}}}}$$

$$u_R = f(\gamma)\frac{A_t}{A_R}\frac{P_0}{\rho_R\sqrt{RT_0}} \qquad \rho_R = \frac{P_\infty}{RT_0} \qquad V_0^* = \frac{V_0}{L^3}$$

N_3 is related to the drag force by blowdown gas and N_4 represents blowdown time. N_5 is similar to Kutateladze number and N_6 is related to entrainment.

The melt dispersal fractions are shown in Fig. 6 to Fig. 9 in terms of the four nondimensional parameters. Since the nondimensional number N_3 is inversely related to the gas Reynolds number, the dispersed fraction decreases as N_3 increases as shown in Fig. 6. The increase of N_4, which means the increase of blowdown time, enhances the dispersed fraction as shown in Fig. 7. N_5 shows the relation between the gravitational force and drag force. Burgles et al. [11] suggested $N_5 = 10$ as a reasonable criterion for the onset of flooding or flow reversal for an annular flow in a vertical tube. It has been also suggested that this criterion could

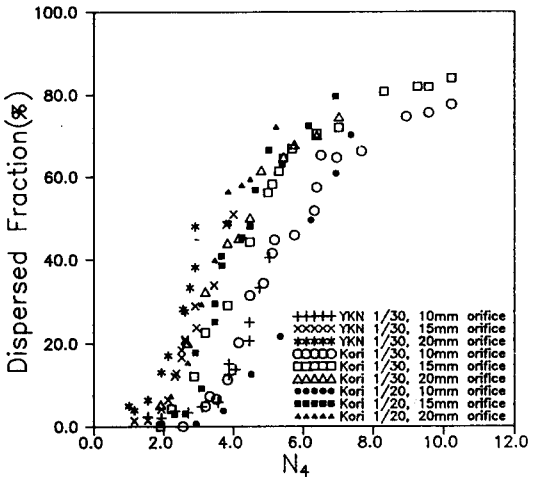

Fig. 7. Dispersed Fraction vs. Nondimensional Number N_4

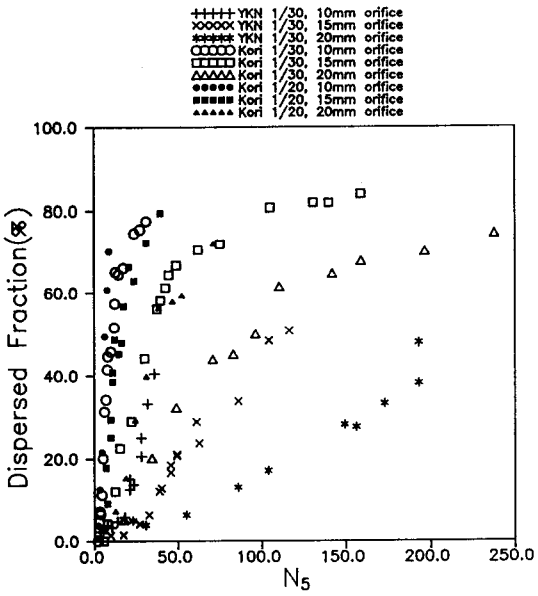

Fig. 8. Dispersed Fraction vs. Nondimensional Number N_5

be used for predicting the onset of debris dispersal in a reactor cavity as shown in Fig. 8. The dispersed fraction also increases as N_6 which is related to the entrainment phenomenon. Ishii et al. [12] suggested $N_6=1.0$ as the inception criterion for droplet entrainment in a two-phase concurrent film flow. However, since then, it has been suggested that this number must be reduced. Fig. 9 shows the relation between the dispersed fraction and N_6. In this figure, it is interesting to note that the dispersion initiates at around $N_6=0.5$.

3.3. Correlation of Dispersal Fraction

In the previous two sections, the measured dispersal fractions of melt were presented with both the key initial conditions and nondimensional parameters in order to characterize the effects of these factors on the dispersal mechanisms. In these analyses, blowdown time and entrainment mechanism (N_6)are found to be the key variables. Based on these observations, an attempt was

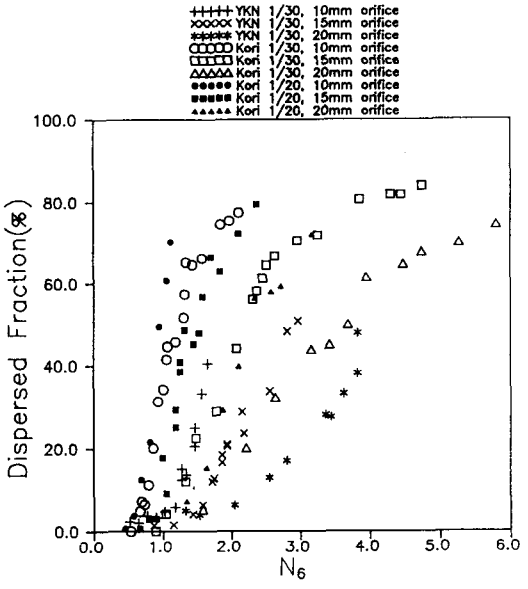

Fig. 9. Dispersed Fraction vs. Nondimensional Number N_6

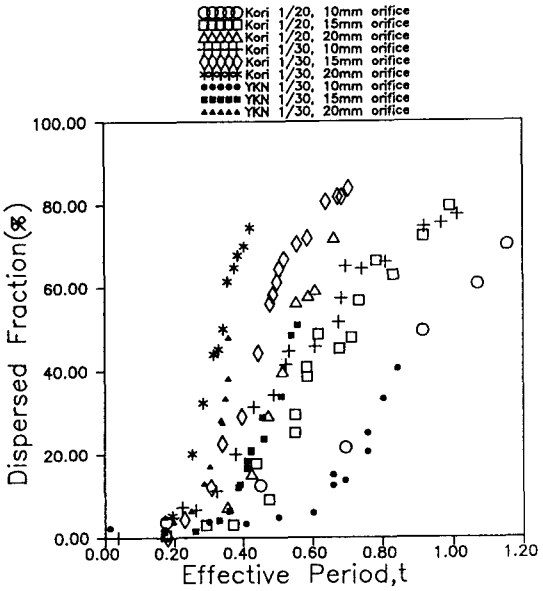

Fig. 10. Dispersed Fraction vs. Effective Period (N6〉 0.5)

made to interpret the experimental data in terms of "effective period", t. The effective period is defined as the blowdown time until the vessel pressure decreases to the pressure which corresponds to $N_6=0.5$. This value of 0.5 for N_6 is based on the cut-off value as shown in Fig. 9. The experimental data are shown in terms of the effective period in Fig.10.

The scatter of the data in this figure is further reduced by introducing a nondimensional effective period,t*, taking into account of the effects of the flight length of droplets and the droplet velocity.

$$t^* = \frac{tv}{L_P} \tag{5}$$

The droplet velocity, v, is assumed to be equal to the blowdown gas velocity and the average value during the effective period is used. Lp is the flight length of droplets as shown in Fig.12. The melt dispersal fractions in terms of this nondimensional effective period are shown in Fig.11 and are best represented by the following correlation.

Dispersed Fraction (%)

$$\begin{cases} = -2.55 + 2.4t & \text{for } 1.0 < t^* < 34 \\ = 80 & \text{for } 34 < t^* \end{cases} \quad (6)$$

This correlation is based on the present test results in the range of N_6 from 0.5 to 6.0. If a droplet is initiated at the point A in Fig. 12, the non-dimensional effective period is 1.0 which is needed for the droplet to fly from the point A to the exit of the cavity. In the present experiments, the dispersion starts at $t^*=1$ and the dispersed fraction rarely exceeded 80%. The remainder of about 20% of the initial melt mass was left in the cavity and other structures.

The validity of this correlation was also tested using the data of different blowdown gases. These additional gases were CO_2 and He and tests were conducted using 1/30-scale Kori cavity. The results are shown in Fig.13 and show that the data are well represented by the correlation.

3.4. Comparison with KAIST and BNL data

To further check the validity of the correlation

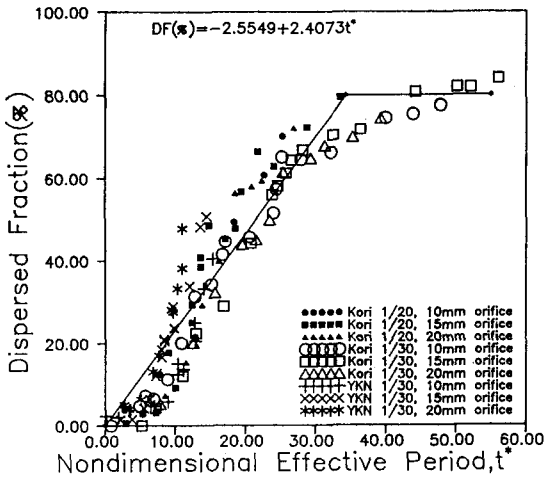

Fig. 11. Dispersed Fraction vs. Nondimensional Effective Period (t*)

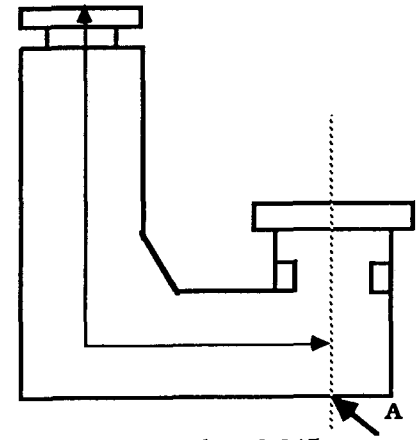

(1) Young-Kwang unit 3&4 1/30 scale cavity

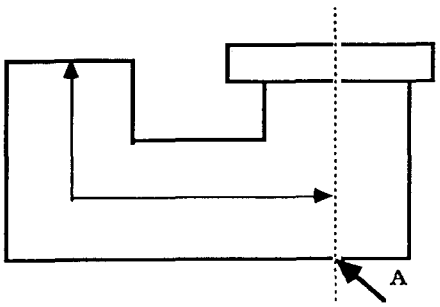

(2) Kori unit 1&2 1/20 scale cavity
* ( ) : Kori 1/30 scale

Fig. 12. Flight Length of Cavity Models

of melt dispersal fraction developed in the present study, the data of KAIST [6, 7] and BNL experiments [3] were analyzed using the parameter of nondimensional effective period. It is noted that both water and Woods metal were used as melt simulant in these experiments. The initial condi-

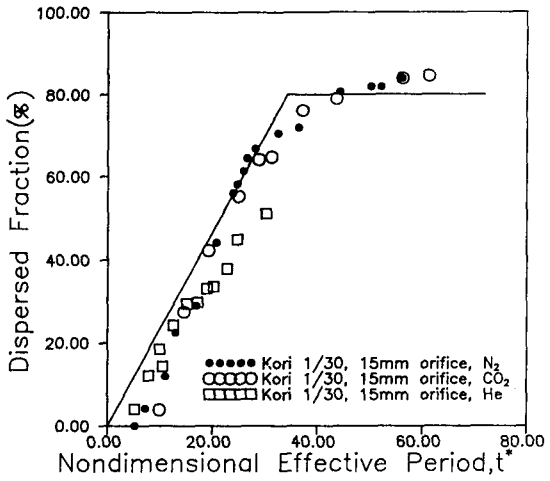

Fig. 13. Dispersed Fraction vs. Nondimensional Effective Period (t*) in Kori 1/30-scale

tions are summarized in Table 2.

Fig. 14 and Fig. 15 shows the comparison of the KAIST, BNL, and the current data together with the proposed correlation. Noting that the cavity geometry and scale and the driving gas are different in these three experiments, the correlation developed in this study based on the nondimensional effective period appears to reasonably predict the amount of melt dispersed from the cavity in direct containment heating events.

Table 2. Initial Conditions of Experiments in KAIST

Initial Conditions	Experimental Cavity Model	
	YKN 1/25th	YKN 1/41th
Pressure of the primary System (MPa)	0.3–5.0	0.3–5.0
Containment Pressure (MPa)	0.1	0.1
Mass of the Core Melt Simulant (kg)	1.2	0.27
Temperature of the Core Melt (K)	298	298
Driving Gas	N_2	N_2
Temperature of the Driving Gas (K)	300	300
Volume of the Driving Gas (m^3)	0.0348	0.0079
Diameter of the Breach Size (mm)	9.42/12.71/16.08	5.70/7.78/9.76
Flight Length(L_p) (m)	0.8925	0.5442
Area(A_R) (m^2)	1.49E-2	5.48E-3

Note : The cavity models are the YKN unit 1&2.

4. Conclusion

An experimental study of direct containment heating phenomena has been conducted using scaled models of Kori 1 and 2 and Young Kwang 3 and 4 cavities. Water was used as melt simulant and the measurement of melt dispersal from the cavity and visual observations of flow field in the cavity tunnel were made with various initial vessel pressures and breach sizes.

It is observed that higher initial pressure and larger breach size enhances the melt dispersal fraction. The cut-off pressure exists below which no melt is dispersed from the cavity. Also, the cavity geometry appears to greatly affect the dispersal rate. This implies that modification of cavity geometry could suppress DCH. Based on the observation of the key parameters such as blowdown time and effective period, a simple correlation of melt dispersal fraction was developed by introducing a nondimensional effective period. This correlation shows good representation of both the data in the present study as well as KAIST and BNL data. For further verification and

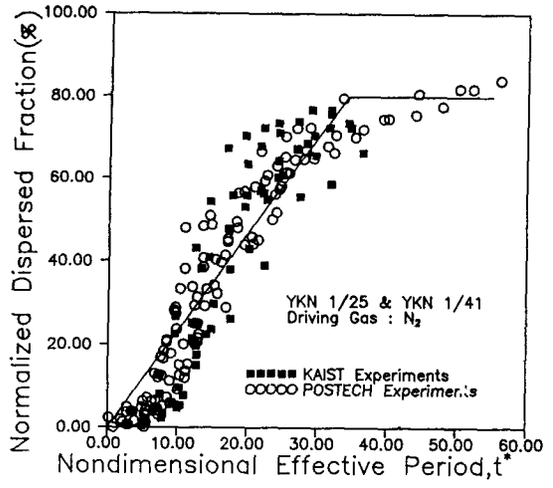

Fig. 14. Application of Correlation to the KAIST Experiments

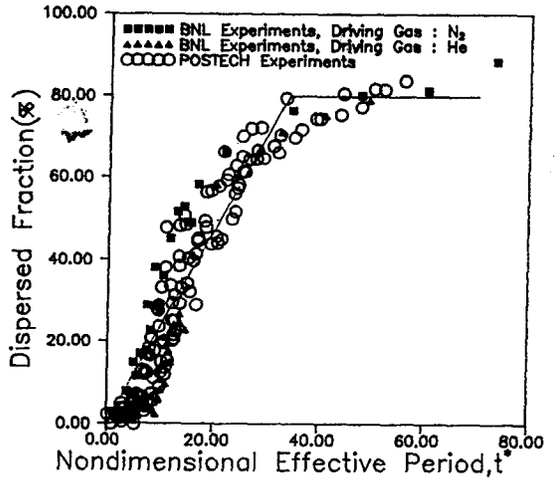

Fig. 15. Application of Correlation to the BNL Experiments

improvement of the correlation, heated melt tests with heavier material are recommended for future study.

References

1. B. W. Spencer, D. Kilsdonk and J. J. Sicenicki, "Phenomenological Investigations Following Postulated Vessel Melt-through", Proceedings of international meeting on thermal nuclear reactor safety, NUREG/CP-0027-V2 part 1 of 2, ANL, 1982
2. N. K. Tutu, et al, "Debris Dispersal from Reactor Cavities during High Pressure Melt Ejection Accident Scenarios", NUREG/CR-5146, BNL,1988.
3. N. K. Tutu, T. Ginsberg, et al. "Melt Dispersal Characteristics of the Watts Bar Cavity", BNL, 1990.
4. Michael D. Allen, Martin Pilch, Richard O. Griffith, David C. William, Robert T. Nichols, "The Third Integral Effects Test (IET-3) in the Surtsey Test Facility", SAND92-0166, SNL, 1992.
5. Michael D. Allen, Martin Pilch, Richard O. Griffith, Robert T. Nichol, "Experiments to Investigate the Effect of Water in the Cavity on Direct Containment Heating (DCH) in the Surtsey Test Facility", SAND91-1173, SNL, 1992.
6. C. S. Lee, "An Experimental Investigation of the High Pressure Melt Ejection from Two Different Scaled Reactor Cavities", M. Thesis, KAIST, 1991.
7. Dong-Sup So, "Experimental and Theoretical Studies on the High Pressure Melt Ejection from a Reactor Pressure vessel", Ph. D. Thesis, KAIST, 1992.
8. K. D. Bergeron, et al., "Development and Application of the Interim Diect Model for the CONTAIN Computer Code", Proceeding 14th WRSI Meeting, Gaithersburg MD, 1986.
9. M. L. Corradini, M. H. Kim, et al., "Application of a Direct Heating Model to Sandia Surtsey Tests", UWRSR-50, University of Wisconsin, 1986.
10. M. H. Kim, "The Effect of multi-volume calculations with a Direct Heating Model to Sandia Surtsey Tests", ANS Transactions, Vol. 56, pp 409, 1988
11. Bergeles. A. E, et al, Two-Phase Flow and

Heat Transfer in the Power and Process Industries, Hemishere Publishing Corporation, pp. 31–33. 1981.

12. M. Ishii and M. A. Grolmes, "Inception Criteria for Droplet Entrainment in Two Phase Concurrent Film Flow", *AIChE Journal*, Vol. 21, No. 2, pp 308–317, 1975.